Research Paper
J. Astron. Space Sci. 35(1), 47-54 (2018)
https://doi.org/10.5140/JASS.2017.35.1.47

JASS Journal of Astronomy and Space Sciences

Solar Insolation Effect on the Local Distribution of Lunar Hydroxyl

Suyeon Kim[1], Yu Yi[1†], Ik-Seon Hong[1,2], Jongdae Sohn[2]

[1]Department of Astronomy, Space Science and Geology, Chungnam National University, Daejeon 34134, Korea
[2]Korea Astronomy and Space Science Institute, Daejeon 34055, Korea

Moon mineralogy mapper (M^3)'s work proved that the moon is not completely dry but has some hydroxyl/water. M^3's data confirmed that the amount of hydroxyl on the lunar surface is inversely related to the measured signal brightness, suggesting the lunar surface is sensitive to temperature by solar insolation. We tested the effect of solar insolation on the local distribution of hydroxyl by using M^3 data, and we found that most craters had more hydroxyl in shade areas than in sunlit areas. This means that the local distribution of hydroxyl is absolutely influenced by the amount of sunshine. We investigated the factors affecting differences in hydroxyl; we found that the higher the latitude, the larger the difference during daytime. We also measured the pyroxene content and found that pyroxene affects the amount of hydroxyl, but it does not affect the difference in hydroxyl between sunlit and shaded areas. Therefore, we confirmed that solar insolation plays a significant role in the local distribution of hydroxyl, regardless of surface composition.

Keywords: lunar hydroxyl distribution, lunar crater, solar insolation

1. INTRODUCTION

For a long time many people assumed the Moon has no water. Although water was detected in some of the lunar samples gathered by the Apollo mission, it was thought to be due to contamination from Earth. However, since satellite remote sensing technology has been applied to lunar exploration, a wider variety of data have been obtained, and we now have intriguing results for lunar water. The Clementine mission posed the possibility of water-ice in permanently shadowed regions (PSRs) (Nozette et al. 1996), and neutron spectrometers mounted on Lunar Prospector and lunar reconnaissance orbiter (LRO) confirmed that the hydrogen was concentrated in the Moon's polar regions (Feldman et al. 1998; Litvak et al. 2012). The lunar crater observation and sensing satellite (LCROSS) confirmed the presence of various volatiles, including water, by performing collision experiments on a hydrogen-rich PSR, the Cabeus crater (Colaprete et al. 2010). In addition, the moon mineralogy mapper (M^3), an infrared spectrometer on Chandrayaan-1, the visual and infrared mapping spectrometer (VIMS) on Cassini, and high-resolution instrument (HRI-IR) on Deep Impact confirmed the absorption features of hydrous components in all regions of the Moon, not only in the polar regions (Clark 2009; Pieters et al. 2009; Sunshine et al. 2009). The morphological feature of the lunar pit craters and its contribution to the diurnal brightness change have been studied for identifying the lava tubes (Hong et al. 2014; Jung et al. 2014; Hong et al. 2015; Jung et al. 2016).

It is believed that most of the hydroxyl present on the lunar surface observed by M^3 is generated from the implantation of solar wind protons (Zeller et al. 1966; Managadze et al. 2011). Hydroxyl formed by the combination of protons and lunar surface oxygen reacts sensitively to Moon's surface temperature because it is connected with a weak bonding force (McCord et al. 2011). As a result of these properties, the distribution of hydroxyl increases at high latitudes with lower temperatures (Clark 2009; Pieters et al. 2009; Sunshine et al. 2009) and tends to increase in the morning and evening rather than at midday (Sunshine et al. 2009; Li & Milliken 2017; Wöhler et al. 2017). In addition to this latitudinal trend and diurnal cycle, hydroxyl also has a local distribution due to lunar topography (Clark 2009; Pieters et al. 2009; Sunshine et al. 2009).

Received 25 FEB 2018 **Revised** 7 MAR 2018 **Accepted** 8 MAR 2018
†**Corresponding Author**
Tel: +82-42-821-5468, E-mail: euyiyu@cnu.ac.kr
ORCID: https://orcid.org/0000-0001-9348-454X

We tested whether solar insolation plays an important role in the local distribution of hydroxyl on the lunar surface because studying the distribution of lunar hydroxyl/water is significant for understanding its characteristics. In this study, we compared the amount of hydroxyl in shade and sunlit areas for 144 craters to identify the influence of solar insolation on hydroxyl. In addition, we examined the latitudinal tendency and divided the data into midday and morning/evening to determine the effects of latitude and local time on the difference in hydroxyl between sunlit and shaded areas. Furthermore, we analyzed the amount of pyroxene to confirm its influence because previous studies have reported that the composition of the Moon's surface also affects the distribution of hydroxyl/water (Cheek et al. 2011; McCord et al. 2011).

2. DATA AND METHODS

M^3 reflectance data were used to analyze hydrated minerals on the lunar surface. The M^3 is a NASA-supported guest instrument on Chandrayaan-1, India's first mission to the Moon. The M^3 is an instrument that maps the surface mineralogy of the Moon in geologic context. These data provide indepth information about geological processes. M^3 is an imaging spectrometer that acquired data through 86 spectral channels from 430 to 3,000 nm (Green et al. 2011).

The spectra which M^3 has acquired had absorption features near 3 μm, depended on hydroxyl and water molecules on the lunar surface (Clark 2009; Pieters et al. 2009; Sunshine et al. 2009). The absorption feature is stronger if more hydroxyl is in that area. Using this feature, we measured the relative amount of hydroxyl on the lunar surface. We hypothesized that more hydroxyl would be distributed in shade areas than in sunlit areas, and to confirm this, we compared and analyzed the absorption features of the sunlit and shade areas. For getting the distribution of hydroxyl, we specified the sunlit areas (red in Fig. 1) and the shade areas (green in Fig. 1) respectively, and we estimated a band ratio of 2.8 μm in reflectance using the formula b76/b81 for each area. The variable b81 (2,816.5000 nm) is the point at which the hydroxyl absorption feature exists, and b76 (2,616.8799 nm) is an ordinary point where no absorption feature exists. Therefore, by calculating b76/b81, we could identify a hydroxyl absorption feature and calculate its depth. We recorded this value as the relative amount of hydroxyl. In this way, we analyzed the 144 craters at 16 M^3 data strips.

We also analyzed the effects of latitude on the difference between sunlit areas and shade areas by classifying the craters according to latitude. To prevent other characteristics affecting the result, we grouped the craters together with similar sun-zenith angles. This means that the craters in the same group were scanned at a similar time zone. One group's data had a sun-zenith angle of 48° to 51° at the equator. These data were taken during the morning or evening. A total of 44 data points were in this group. Another group's data had a sun-zenith angle of 12° to 14° at the equator. A total of 64 craters data points were in this group, and these data were taken near midday.

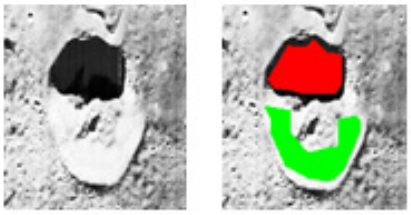

(a) (b)

Fig. 1. Spectrometer images of a lunar crater. Fig. 1(b) is same crater as Fig. 1(a) but we designated the shade area (red) and the sunlit area (green) of the crater separately and measure the amount of hydroxyl.

We also measured the pyroxene content and analyzed the influence on hydroxyl in sunlit areas and shadowy areas. We used the method of integrated band depth (IBD) at 1,000 nm to analyze the amount of pyroxene (Staid et al. 2011). To prevent other features affecting the results, we divided the group by sun-zenith angle, as described above.

3. RESULTS AND DISCUSSION

3.1 Hypothesis 1: More Hydroxyl is Distributed in Areas with Less Solar Illumination

Our first hypothesis was that there is more hydroxyl in shade areas than sunlit areas. Analysis of the characteristics of the hydroxyl component in sunlit areas and shade areas revealed that the amount of hydroxyl was higher in shade areas than sunlit areas in almost all craters studied, except a few craters (Fig. 2). Only Four craters had lower amounts of hydroxyl in shade areas than in sunlit areas. These results support our first hypothesis. This implies that the hydroxyl formed by implantation of solar wind protons is less active in shade areas because the kinetic energy of the molecules increases at high surface temperatures.

3.2 Hypothesis 2: The Effects of Latitude on Hydroxyl are Different Between Sunlit and Shade Areas

On the Moon, the shape of shade is affected by latitude. In low latitudes, the sun shines almost vertically, so the

shade area is smaller, but at high latitudes it becomes obliquely shaded, so the shade area is larger and clearer. Also, at high latitudes, the shadows lean in a polar direction do not receive many hours of sunlight, so there are many areas that continue to remain in shade. Based on these facts, we hypothesized that differences in the amount of hydroxyl in shade and sunlit areas at higher latitudes will be greater than at low latitudes. We arranged the data according to latitude to test this hypothesis (Fig. 3). To prevent other factors from affecting the results, we grouped the data by sun-zenith angle.

When the sun-zenith angle was 12° to 14° at the equator, the differences in hydroxyl between shade and sunlit areas increased gradually as latitude increased. Correlation coefficients and p-values were calculated using the R program's cor.test package. The correlation coefficient was 0.603807 and the p-value was 1.279e-07, confirming a correlation. When the sun-zenith angle was 48° to 51°, there was almost no significant correlation. This result means that the differences in the amount of hydroxyl with latitude was more noticeable during midday than in the morning and evening, likely due to the small differences in hydroxyl in shadow regardless of whether the latitude was low or high. Thus, our second hypothesis was supported only for daytime.

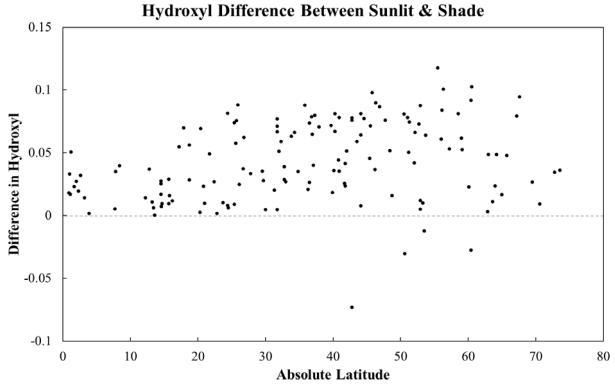

Fig. 2. Differences in the amount of hydroxyl between sunlit and shade areas. The x-axis represents the absolute value of the latitude and the y-axis represents the differences in hydroxyl. It was calculated as $(\frac{b76}{b81})_{shadow}$-$(\frac{b76}{b81})_{sunlit}$. The number of craters is 144.

3.3 Hypothesis 3: The Pyroxene Content of the Lunar Surface Affects the Difference in the Amount of Hydroxyl in Shade and Sunlit Areas

Previous studies have shown that the amount of hydroxyl depends on the amount of pyroxene on the lunar surface (McCord et al. 2011). To test pyroxene's effect on the difference in the amount of hydroxyl between sunlit and shaded areas, we compared the influence of pyroxene on hydroxyl between these areas during midday and morning/evening (Fig. 4). The results showed that the amount of hydroxyl decreased when the amount of pyroxene increased, regardless of local time, and there was no correlation between the amount of pyroxene and the difference in the amount of hydroxyl between sunlit and shaded areas. These results imply that surface composition does not affect the differences in hydroxyl between sunlit areas and shade areas, although the surface composition affects to amount of hydroxyl in general. Therefore, our third hypothesis was not supported.

Although we classified our study regions and analyzed data by controlling solar insolation and surface composition, there is an unsolved problem in this study. We employed M^3 data provided by the photothermal deflection spectroscopy (PDS) and the residual thermal emissions of the lunar surface effect near 3 μm of the data, due to incomplete thermal removal

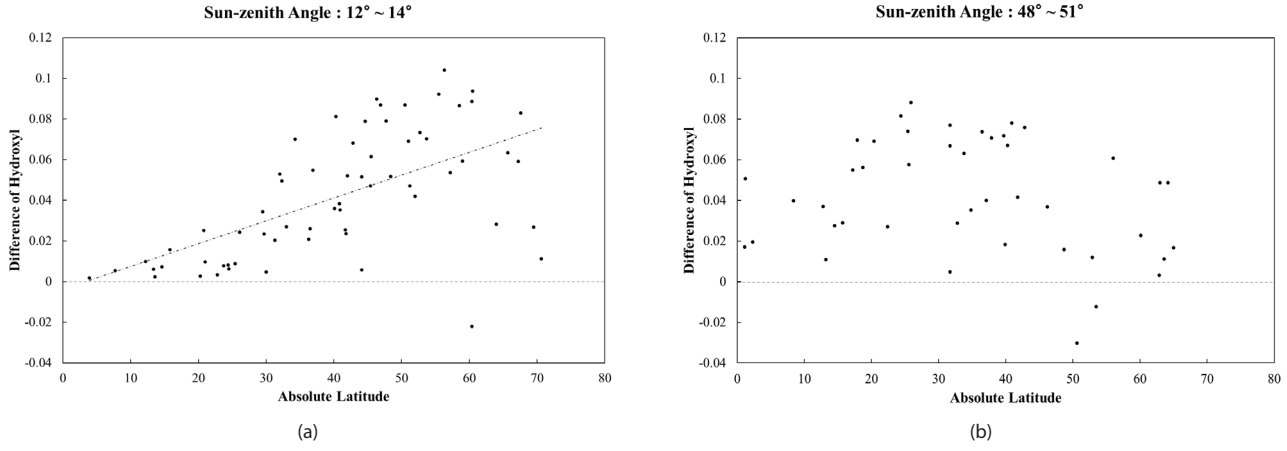

Fig. 3. Difference in hydroxyl by latitude when the sun-zenith angle was approximately (a) 12°–14° and (b) 48°–51°. The x-axis represents the absolute value of latitude and the y-axis represents the differences in hydroxyl between shade and sunlit areas.

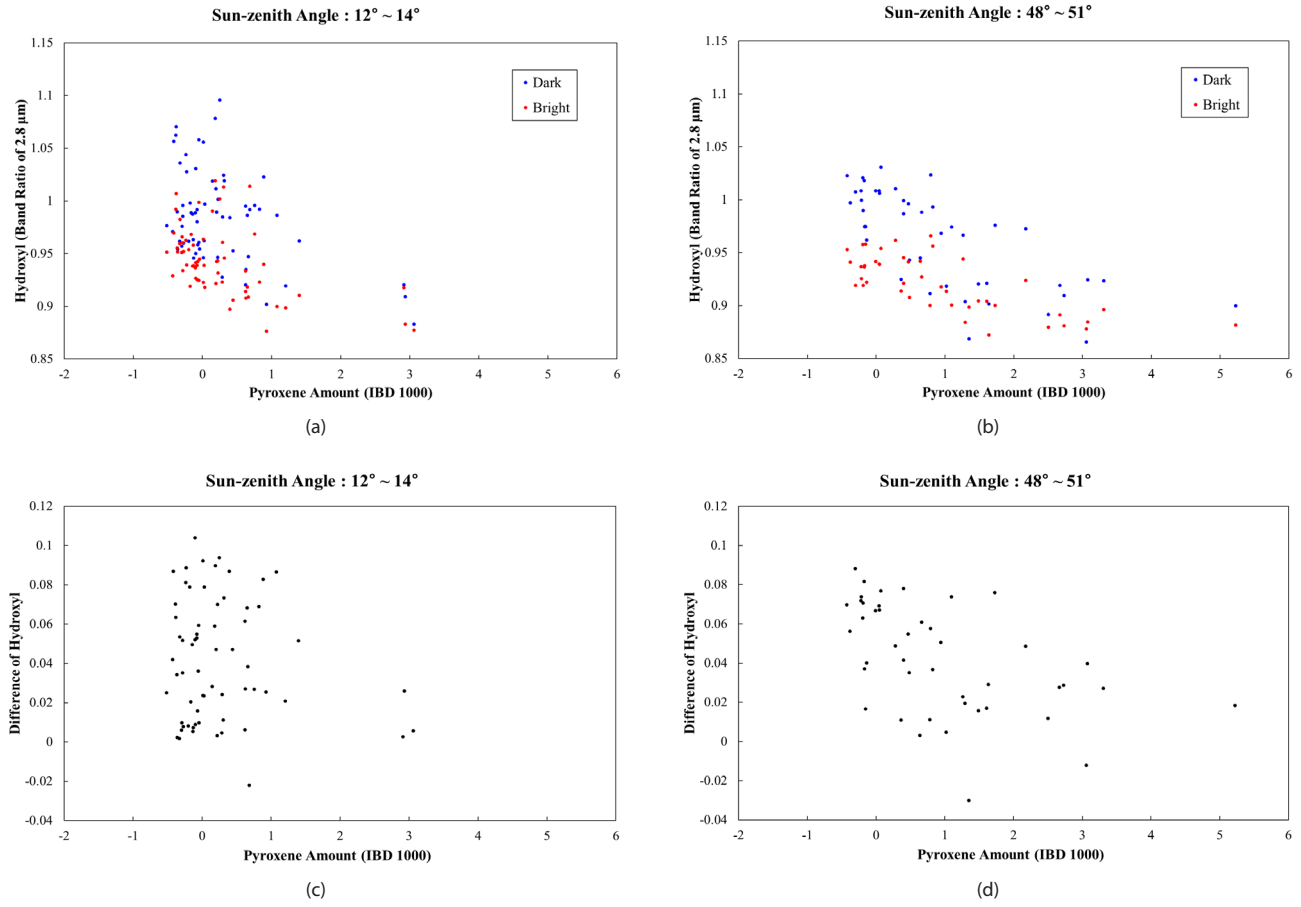

Fig. 4. The amount of hydroxyl and the amount of pyroxene during (a) midday and (b) morning and evening. The x-axis represents the pyroxene content, and the y-axis represents the amount of hydroxyl. The red points are sunlit areas, and the blue points are shade areas. The difference in hydroxyl and the amount of pyroxene during (c) midday and (d) morning and evening. The y-axis represents the difference in hydroxyl between shade and sunlit areas. The x-axis pyroxene amount value is calculated of the area of the absorption band of the spectral reflectance. Therefore, this pyroxene amount should be considered as the approximation of relative amount. The negative number of pyroxene value appears due to the error of simplified fitting in absorption estimation.

(Li & Milliken 2016; Wöhler et al. 2017). We plan to conduct further studies to consider thermal removal.

4. CONCLUSIONS

Since hydroxyl groups on the lunar surface are affected by temperature, the distribution of hydroxyl not only shows a latitudinal tendency and diurnal cycle, but it is also affected locally by changes in the amount of sunshine due to topography. We selected 144 craters to characterize this local distribution of hydroxyl, and we then compared the distribution of hydroxyl in sunlit and shade areas of the craters. As a result, we observed that 97 % of the data used in this study had a larger amount of hydroxyl in shade areas than in sunlit areas in each crater. This means that the local distribution of hydroxyl is absolutely influenced by the amount of sunshine. Furthermore, we tested the effects of latitude, local time, and other components on these differences, and we found that the higher the latitude, the greater the difference, and the effect of latitude was more pronounced at midday than during the morning/evening. This also suggests the local distribution of hydroxyl is greatly affected by differences in the amount of sunshine. The differences in surface composition did not affect the difference in the amount of hydroxyl in sunlit and shade areas, but we confirmed that the amount of hydroxyl decreased as the amount of pyroxene increased. Thus, we found that the local distribution of hydroxyl is absolutely influenced by differences in the amount of sunshine on the lunar surface.

ACKNOWLEDGMENTS

This research was supported by Basic Science Research Program through the National Research Foundation of

Korea (NRF) funded by the Ministry of Education (NRF-2016 R1D1A3B03933339).

REFERENCES

Cheek LC, Pieters CM, Boardman JW, Clark RN, Combe JP, et al., Goldschmidt crater and the Moon's north polar region: results from the moon mineralogy mapper (M3), J. Geophys. Res. 116, E00G02 (2011). https://doi.org/10.1029/2010JE003702

Clark RN, Detection of adsorbed water and hydroxyl on the Moon, Science 326, 562-564 (2009). https://doi.org/10.1126/science.1178105

Colaprete A, Schultz P, Heldmann J, Wooden D, Shirley M, et al., Detection of water in the LCROSS ejecta plume, Science 330, 463-468 (2010). https://doi.org/10.1126/science.1186986

Feldman WC, Maurice S, Binder AB, Barraclough BL, Elphic RC, et al., Fluxes of fast and epithermal neutrons from Lunar Prospector: Evidence for water ice at the lunar poles, Science 281, 1496-1500 (1998). https://doi.org/10.1126/science.281.5382.1496

Green RO, Pieters C, Mouroulis P, Eastwood M, Boardman J, et al., The moon mineralogy mapper (M^3) imaging spectrometer for lunar science: Instrument description, calibration, on-orbit measurements, science data calibration and on-orbit validation, J. Geophys. Res. 116, E00G19 (2011). https;//doi.org/10.1029/2011JE003797

Jung J, Yi Y, Kim E, Identification of martian cave skylights using the temperature change during day and night, J. Asron. Space Sci. 31, 141-144 (2014). https://doi.org/10.5140/JASS.2014.31.2.141

Jung J. Hong IS, Cho E, Yi Y, Method for identifying lava tubes among pit craters using brightness profile across pits on the Moon or Mars, J. Astron. Space Sci. 33, 21-28 (2016). https://doi.org/10.5140/JASS.2016.33.1.21

Hong IS, Yi Y, Kim E, Lunar pit craters presumed to be the entrances of lava caves by analogy to the Earth lava tube pits, J. Astron. Space Sci. 31, 131-140 (2014). https://doi.org/10.5140/JASS.2014.31.2.131

Hong IS, Yi Y, Yu J, Haruyama J, 3D modeling of Lacus Mortis pit crater with presumed interior tube structure, J. Astron. Space Sci. 32, 113-120 (2015). https://doi.org/10.5140/JASS.2015.32.2.113

Li S, Milliken RE, An empirical thermal correction model for moon mineralogy mapper data constrained by laboratory spectra and diviner temperatures, J. Geophys. Res. 121, 2081-2107 (2016). https://doi.org/10.1002/2016JE005035

Li S, Milliken RE, Water on the surface of the Moon as seen by the moon mineralogy mapper: distribution, abundance, and origins, Sci. Adv. 3, e1701471 (2017). https://doi.org/10.1126/sciadv.1701471

Litvak ML, Mitrofanov IG, Sanin A, Malakhov A, Boynton WV, et al., Global maps of lunar neutron fluxes from the LEND instrument, J. Geophys. Res. 117, E00H22 (2012). https://doi.org/10.1029/2011JE003949

Managadze GG, Cherepin VT, Shkuratov YG, Kolesnik VN, Chumikov AE, Simulating OH/H2O formation by solar wind at the lunar surface, Icarus 215, 449-451 (2011). https://doi.org/10.1016/j.icarus.2011.06.025

McCord TB, Taylor LA, Combe JP, Kramer G, Pieters CM, Sources and physical processes responsible for OH/H_2O in the lunar soil as revealed by the moon mineralogy mapper (M^3), J. Geophys. Res. 116, E00G05 (2011). https://doi.org/10.1029/2010JE003711

Nozette S, Lichtenberg CL, Spudis P, Bonner R, Ort W, et al., The clementine bistatic radar experiment, Science 274, 1495-1498 (1996). https://doi.org/10.1126/science.274.5292.1495

Pieters CM, Goswami JN, Clark RN, Annadurai M, Boardman J, et al., Character and spatial distribution of OH/H2O on the surface of the Moon seen by M^3 on Chandrayaan-1, Science 326, 568-572 (2009). https://doi.org/10.1126/science.1178658

Staid MI, Pieters CM, Besse S, Boardman J, Dhingra D, et al., The mineralogy of late stage lunar volcanism as observed by the moon mineralogy mapper on Chandrayaan-1, J. Geophys. Res. 116, E00G10 (2011). https://doi.org/10.1029/2010JE003735

Sunshine JM, Farnham TL, Feaga LM, Groussin O, Merlin F, Temporal and spatial variability of lunar hydration as observed by the Deep Impact spacecraft, Science 326, 565-568 (2009). https://doi.org/science.1179788

Wöhler C, Grumpe A, Berezhnoy AA, Shevchenko VV, Time-of-day–dependent global distribution of lunar surficial water/hydroxyl, Sci. Adv. 3, e1701286 (2017). https://doi.org/10.1126/sciadv.1701286

Zeller EJ, Ronca LB, Levy PW, Proton-induced hydroxyl formation on the lunar surface. J. Geophys. Res. 71, 4855-4860 (1966). https://doi.org/10.1029/JZ071i020p04855

APPENDIX

Table 1. List of craters used for data analysis

Crater name	Longitude (°)	Latitude (°)	Sun-zenith (°)	Diameter (km)	Pyroxene	Shadowy region	Sunlit region
unnamed crater	359.3	64.2	73.6	4.4	2.17415	0.972565	0.923882
piton A	359.1	39.9	60.6	5.3	5.223071	0.899867	0.88152
Archimedes C	358.5	31.7	57.5	7.7	1.018864	0.918414	0.913621
Marco Polo B	358.1	17.2	53.2	6.4	0.467036	0.996143	0.941256
W. Bond D	3.2	63.6	72.6	6.8	0.780607	0.911505	0.9003
Bruce	0.4	1.2	51	6.1	0.944245	0.968411	0.917785
unnamed crater	4.3	53.3	52.5	3.6	2.497867	0.886725	0.876642
W. Bond B	7.5	65	73.8	15.2	-0.155527	0.974709	0.95802
Archytas U	9.2	62.9	72.2	7.4	0.639509	0.945174	0.942003
Protagoras	7.3	56	68.3	21.1	0.661553	0.988105	0.927271
Egede B	9	50.6	65.3	7.3	1.351483	0.868533	0.89867
Cassini C	7.8	41.8	60.9	13.8	0.399328	0.9869	0.945355
Cassini F	7.3	40.9	60.5	6.7	0.399477	0.999269	0.921157
Calippus A	7.9	37.1	58.9	15.7	-0.139311	0.962088	0.921987
Manilius D	7	13.2	51.1	4.7	0.364198	0.924702	0.91377
Aristoteles M	27.3	53.5	66.5	7	3.056768	0.865692	0.877853
Aristoteles N	26.8	52.9	66.4	5.3	2.502322	0.891418	0.879532
Plana C	27.1	42.8	60.6	13.7	1.727608	0.975982	0.900055
Posidonius G	27.2	34.8	56.7	4.8	0.481332	0.94308	0.90792
Posidonius F	27.1	32.8	55.9	6	2.730562	0.909608	0.880859
Borel	26.4	22.4	52.5	4.7	3.309365	0.923392	0.896276
Maskelyne G	26.7	2.3	48.6	5.8	1.290837	0.903721	0.884209
Beaumont B	26.8	-18.7	51.1	15.1	-0.37821	0.997265	0.941019
Polybius E	26.2	-24.4	53.4	8.2	-0.175216	1.018019	0.936438
Polybius B	25.5	-25.6	54.4	12	0.790079	1.023521	0.965833
Lindenau E	26.5	-31.7	55.9	7.4	-0.009177	1.008421	0.941597
Riccius M	26.5	-37.9	58.7	13.7	-0.187279	0.98995	0.919264
Democritus B	28.6	60.1	70.3	11.7	1.263634	0.966806	0.943975
Jansen D	28.5	15.7	49.7	6.7	1.636166	0.901429	0.872414
Jansen E	27.8	14.5	50	6.6	2.667699	0.919006	0.891346
Beaumont G	27.1	-20.4	52.1	7.7	0.04421	1.008393	0.93925
Lindenau E	26.5	-31.7	56.6	7.4	0.067369	1.030938	0.954029
Aristoteles N	26.9	52.9	64.6	5.3	2.894226	0.889117	0.88404
Plana C	27.1	42.8	58.4	13.7	1.506411	0.898062	0.971123
Posidonius F	27.1	32.8	53	6	2.778917	0.941724	0.902901
Posidonius A	29.5	31.7	50.6	11.1	0.286752	1.000588	0.929308
Clerke	29.8	21.7	45.8	6.7	0.355949	0.960035	0.910925
Fabbroni	29.3	18.7	45.2	10.5	2.544127	0.921879	0.893542
Beketov	29.2	16.2	44.5	8.3	1.715198	0.912734	0.901082
Jansen D	28.5	15.7	45	6.7	1.565743	0.917161	0.907707
Jansen L	30.1	14.7	43.2	6.9	1.929314	0.897003	0.887654
Jansen E	27.8	14.5	45.2	6.6	2.76693	0.927139	0.910118
Maskelyne M	27.9	7.8	43.8	7.3	0.659005	0.946787	0.91164
Maskelyne K	29.7	3.2	41.6	5.4	1.406074	0.9114429	0.897184
Maskelyne B	29	2	42.2	8.3	1.206666	0.931557	0.904316
Maskelyne Y	28.2	1.7	43	4.3	0.559096	0.934253	0.911221
unnamed crater	29.3	0.9	41.9	4.1	1.002803	0.920734	0.902592
Censorinus K	28.9	-1	42.3	4.5	1.037425	0.941258	0.908029
Torricelli B	29.2	-2.6	42	6.8	1.587401	0.937386	0.905265
Beaumont L	30	-14.5	43.1	4.2	2.735981	0.953245	0.927961
Piccolomini K	29.7	-25.7	47.5	7.6	0.443102	1.024845	0.949102
Piccolomini W	29.2	-26.8	48.4	5.5	-0.304525	1.024652	0.962404
Riccius Y	29.1	-35.8	52.9	8.9	-0.543325	1.037467	0.949545
Whler C	30.6	-36.8	52.4	11.5	-0.458086	1.00865	0.929996
Whler B	30.8	-37.3	52.6	9.8	-0.397726	1.01311	0.933298
Lockyer A	31	-44.1	56.6	9.6	-0.285683	1.013296	0.932222
Arnold F	35.2	67.6	66.8	10.4	0.886611	1.033772	0.939342
Grtner D	34	58.5	57.8	7.6	1.078036	0.979251	0.89816

Crater name	Longitude (°)	Latitude (°)	Sun-zenith (°)	Diameter (km)	Pyroxene	Shadowy region	Sunlit region
Baily B	35.2	51	50.6	7	0.824552	0.992584	0.914509
Hercules J	36.4	44.1	44.1	7.9	1.398573	0.971669	0.907342
Piccolomini W	29.2	-26.7	29.6	5.5	-0.267678	0.992392	0.955185
Hommel E	31	-59.1	60.9	13.4	0.431375	1.013512	0.961055
Hommel HA	30.6	-52.1	54.1	10.4	0.030436	1.024671	0.958478
Boguslawsky H	29	-72.8	74.2	20.9	0.765868	1.022633	0.988034
Schomberger Z	27.3	-73.6	74.9	6.2	1.683891	1.004166	0.968128
unnamed crater	43.6	48.7	63	6.5	1.487597	0.920316	0.904483
Maury L	42.5	40.3	59.1	4.2	0.049692	1.006214	0.93919
unnamed crater	43.6	36.5	56.5	3.8	1.097212	0.974448	0.900688
Macrobius V	43.3	25.4	52	4.5	-0.212667	0.999475	0.925601
unnamed crater	42.5	12.8	49	7.5	-0.169326	0.974779	0.937756
Secchi U	42.2	1.1	48	4.9	1.606775	0.921212	0.904168
unnamed crater	42.5	-8.4	48.2	3.8	3.076162	0.924416	0.884589
Bohnenberger N	41.9	-17.9	50.7	5.7	-0.424368	1.022814	0.953131
Santbech Z	43	-25.9	52.3	5.4	-0.303103	1.007493	0.919277
Neander Z	42	-33.8	56.4	6.1	-0.196611	1.020688	0.957594
unnamed crater	41.7	-39.7	59.4	5	-0.218389	1.008485	0.936627
Janssen K	42.3	-46.2	62.4	15	0.821989	0.993259	0.956458
Boussingault T	43.1	-63	72.1	19.4	0.281351	1.010369	0.961559
unnamed crater	52.1	56.1	58	7.1	0.043599	1.040128	0.956026
Endymion X	50.1	52.9	52.7	6	0.25769	1.013597	0.925908
Atlas L	48.6	51.3	51	5.4	0.17558	1.014613	0.940082
unnamed crater	49.5	45.8	45.7	4.6	0.594746	1.02887	0.93102
Chevallier K	50.9	43.5	43.9	5.6	0.96012	0.983881	0.92494
Tralles C	49.4	27.8	28.7	7.3	0.052401	0.992194	0.958888
unnamed crater	60.5	51.2	51.4	6	0.203358	0.988659	0.938315
unnamed crater	61.3	45.5	46.1	4.7	0.621775	1.001863	0.93049
unnamed crater	57.7	45.4	45.2	3.6	0.442684	0.953118	0.907402
unnamed crater	58.9	42.8	43	5.6	0.650823	0.99587	0.918045
unnamed crater	59.7	40.8	41.3	4.9	0.664078	0.954169	0.910068
Cleomedes S	58.9	29.5	30.5	7.6	-0.367431	0.989961	0.954607
Cusanus F	73.6	70.6	70.2	12	0.30773	1.021147	1.012068
unnamed crater	71.6	67.2	66.8	4.2	0.184889	1.090133	1.010753
unnamed crater	69.7	60.5	60	6.2	0.249627	1.101066	0.998406
Endymion L	71.4	55.5	55.4	6.9	0.012023	1.074183	0.956566
Endymion M	71	52.7	52.7	9.3	0.317364	1.018287	0.945534
unnamed crater	71	-24.5	28.6	5.3	0.622632	0.920438	0.914383
unnamed crater	71.2	-36.9	40	6.5	-0.077973	0.982446	0.917655
unnamed crater	71.1	-42	44.7	4.5	-0.102584	0.98553	0.934018
unnamed crater	70.7	-44.6	47.2	6	-0.181091	0.99955	0.922126
unnamed crater	72.7	-69.5	71.3	6.5	0.756367	0.998621	0.971809
unnamed crater	80.1	-22.8	27.3	4	0.217786	0.947853	0.946039
Humboldt N	80.6	-26.1	30.6	14.5	0.292755	0.986314	0.96149
unnamed crater	81	-32	35.9	3.8	-0.077051	0.989979	0.938848
unnamed crater	79.9	-32.3	35.7	5.8	-0.145827	0.994119	0.935275
unnamed crater	95.7	65.7	65.8	5	-0.383146	1.065463	1.017539
unnamed crater	93	64	63.8	3	0.146434	1.019122	0.99551
unnamed crater	94.8	60.4	60.8	5.6	0.686057	0.991546	1.018966
unnamed crater	94.5	59	59.3	9	-0.05257	1.058735	0.997079
unnamed crater	94.6	57.2	57.7	5.6	-0.32294	1.038245	0.985186
unnamed crater	93.1	53.7	54.1	3.4	-0.386419	1.059008	0.995119
unnamed crater	92.9	-12.2	20.3	6.4	-0.293888	0.979028	0.964789
unnamed crater	91.9	-13.6	20.6	3.7	-0.360054	0.954153	0.953874
unnamed crater	91.8	-20.8	26.1	6	-0.516109	0.97631	0.952859
Curie K	93	-23.7	29.2	11.1	-0.273559	0.959346	0.949091
unnamed crater	94.1	-29.7	34.7	5	0.025451	0.966793	0.938942
Donner R	92.3	-34.3	38.3	14.9	0.223357	0.997074	0.930872
unnamed crater	92.2	-36.5	40.1	3.6	2.933886	0.909045	0.882551
unnamed crater	91.1	-41.7	44.7	6	0.927561	0.902801	0.877232
unnamed crater	93.4	-44.1	47.5	8.8	3.061002	0.884794	0.87685
unnamed crater	92.7	-47.7	50.6	10.8	0.034115	0.997185	0.921228

Crater name	Longitude (°)	Latitude (°)	Sun-zenith (°)	Diameter (km)	Pyroxene	Shadowy region	Sunlit region
unnamed crater	91.4	-50.5	53	6.8	0.394786	0.982067	0.901223
unnamed crater	93.2	-56.3	38.9	10.1	-0.100375	1.02899	0.928346
unnamed crater	91.4	-60.4	62.6	5.1	-0.230726	1.027875	0.936172
unnamed crater	104.7	46.9	47.9	4.9	-0.415779	1.05663	0.969803
unnamed crater	105	40.9	42.6	5.9	-0.282926	0.995607	0.960347
unnamed crater	103.2	40.3	41.5	5.3	-0.23817	1.043921	0.962691
unnamed crater	104.6	31.3	33.9	5.9	-0.166066	0.988832	0.968447
unnamed crater	104.4	24.4	28	6	-0.20051	0.961825	0.953706
unnamed crater	104.9	20.3	25.1	6.7	2.913248	0.920367	0.91773
unnamed crater	105.7	14.6	21.9	6.9	-0.129005	0.945858	0.93849
unnamed crater	104.6	7.7	17.6	19.1	-0.133222	0.963379	0.957976
unnamed crater	103.3	-3.9	15.9	6.5	-0.331753	0.961651	0.95987
unnamed crater	103.7	-13.4	21.2	8.8	-0.298744	0.957114	0.951015
unnamed crater	103.5	-15.8	22.7	6.6	-0.067058	0.958428	0.942678
unnamed crater	105.5	-21	27.9	6.8	-0.043399	0.954548	0.944838
unnamed crater	104	-25.4	30.7	6.9	-0.09904	0.950294	0.941473
unnamed crater	103.4	-30	34.4	13.7	0.285941	0.9278	0.923127
unnamed crater	103	-33	37	6.9	0.629004	0.934906	0.907844
unnamed crater	104	-36.3	40.2	4.9	1.204287	0.91941	0.898563
unnamed crater	105.3	-40.1	44.1	7.1	-0.054374	0.960689	0.924666
unnamed crater	105.4	-41.8	45.7	5.5	0.013472	0.946266	0.922639
unnamed crater	105.1	-46.3	49.8	3.8	0.193728	1.011468	0.92165
unnamed crater	105.5	-48.4	51.8	3.2	-0.284891	0.985632	0.933826
unnamed crater	102.9	-52	54.6	6.4	-0.429947	0.970903	0.929026